Landscape expressions of tectonics in the Zagros fold-and-thrust belt

Ahmed K. Obaid [1,2], Mark B. Allen [2]

[1] Department of Geology, University of Baghdad, Al-Jadriyh Street, Baghdad, Iraq

[2] Department of Earth Sciences, University of Durham, Durham DH1 3LE, UK

ahamedobaid@gmail.com; m.b.allen@durham,ac.uk

Abstract

This study uses geomorphic indices, including normalized channel steepness index (k_{sn}), integrated relief and hypsometric index (HI), to investigate how landscape responds to tectonic and climatic drivers in the Zagros fold-and-thrust belt, and show how geomorphology can be a sensitive indicator of tectonic processes. There is a broad association of relatively high k_{sn} values (>50 $m^{0.9}$) with the upper elevation limit for seismogenic thrusting, which occurs regionally at the 1250 m topographic contour. Higher k_{sn} values occur beyond this seismicity cut-off in the Bakhtyari Culmination, but are rare in the Fars region. We measured HI values for 17380 third order river basins across the Zagros. In many areas the low/high HI transition (0.3) is typically at the elevation limit of seismogenic thrusting. There are two important exceptions. In the Dezful Embayment/Bakhtyari Culmination the low/high HI transition lies at higher elevations than the thrust seismicity cut-off. In the Fars region, the HI transition lies at lower elevations than the seismicity cut-off. We explain these differences by the different climates of the two areas: wetter conditions and vigorous drainage systems in the Dezful/Bakhtyari region retard orogenic plateau growth; drier climate and low power rivers in the Fars region promote plateau growth. Orographic precipitation may itself have a tectonic control; regional basement strength variations have caused intense thrusting and high relief in the Bakhtyari Culmination. Integrated relief of five across-strike Zagros topographic swath profiles is in the range 2.2 – 2.8 10^8 m^2. We argue that this consistency within ~25% relates to the comparable strain rates across different sectors of the Zagros, regardless of local structural, drainage network or climatic variations.

1. Introduction

The tectonics of the Zagros are far from completely understood, despite it being one of the largest and most active fold-and-thrust belts on Earth (Fig. 1). Information in the present landscape has not been fully analysed to improve tectonic models. Nor do we understand the interactions of landscape, tectonics and climate. In this study we have conducted a range-wide

analysis of geomorphology to improve the current state of knowledge of Zagros tectonics. We hypothesise that geomorphic and structural variations between different regions of the range might correlate with variations in climate, but that the climatic variations might ultimately be controlled by the pre-collisional, basement geology of the Zagros.

One of the major tectonic events of the Cenozoic was the closure of the Neo-Tethys Ocean. A consequence of this closure was the Arabia-Eurasia collision, which initiated the Zagros fold-and-thrust belt as one of the largest and most tectonically active mountain ranges in the world (Mouthereau et al., 2012). It has accommodated part of the Arabia-Eurasia convergence (Blanc et al. 2003; McQuarrie, 2004; Ghasemi and Talbot, 2006; Alavi, 2007) since at least the Early Miocene (Fakhari et al., 2008; Khadivi et al., 2010; Khadivi et al., 2012). The Zagros fold-and-thrust belt deforms both the underlying basement and the overlying folded sedimentary cover of the Arabian Plate (Talebian and Jackson, 2004). The Zagros represents an area with a wide range of exposed geology, but mainly sedimentary rocks from the Jurassic to the Holocene (Fig. 1b).

Whereas there is pronounced crustal deformation within the Zagros, shown by the abundant seismicity and shortening across the range, the Turkish-Iranian Plateau represents a region of the collision zone where there is little active convergence, relatively low relief, and subdued seismicity (mainly strike-slip) (Nissen et al., 2011). The boundary between the plateau and the active fold-and-thrust belt is debatable, but there is a marked cut-off in thrust seismicity at the 1250 m elevation contour (Fig. 1a). Most thrust events are confined to the low elevation part of the Zagros Simply Folded Belt, below the 1250 m elevation contour (Nissen et al., 2011). Elevations continue to climb to the northeast, but with little indication of active shortening, at least at upper crustal levels (Allen et al., 2013). The thrust seismicity cut-off is therefore an important marker for studies of landscape response to tectonism in the Zagros.

Active tectonism has been widely investigated using multiple geomorphic indices because of their ability to detect the landscape response to tectonic drivers (e.g. Lavé and Avouac, 2000; Keller and Pinter, 2002; Zielke at al., 2010). In addition, these indices provide measurements which help assess the relative roles of crustal displacement and the variation in rock resistance during landscape development (e.g. Walcott and Summerfield, 2008). .

The study of river-fold interaction in the Zagros has previously been dealt with by local studies in different parts of the Zagros (e.g. Bahrami, 2013; Bretis et al., 2011; Burberry et al., 2008, 2010; Ramsey et al., 2008; Walker et. al., 2011; Zebari and Burberry, 2015; Obaid and

Allen, 2017). This paper studies the regional landscape response of the Zagros to potential climatic and tectonic drivers. The geomorphic indices used are: hypsometric index (HI) of drainage basins, k_{sn} values, and the integrated topographic relief for across-strike topographic swath profiles.

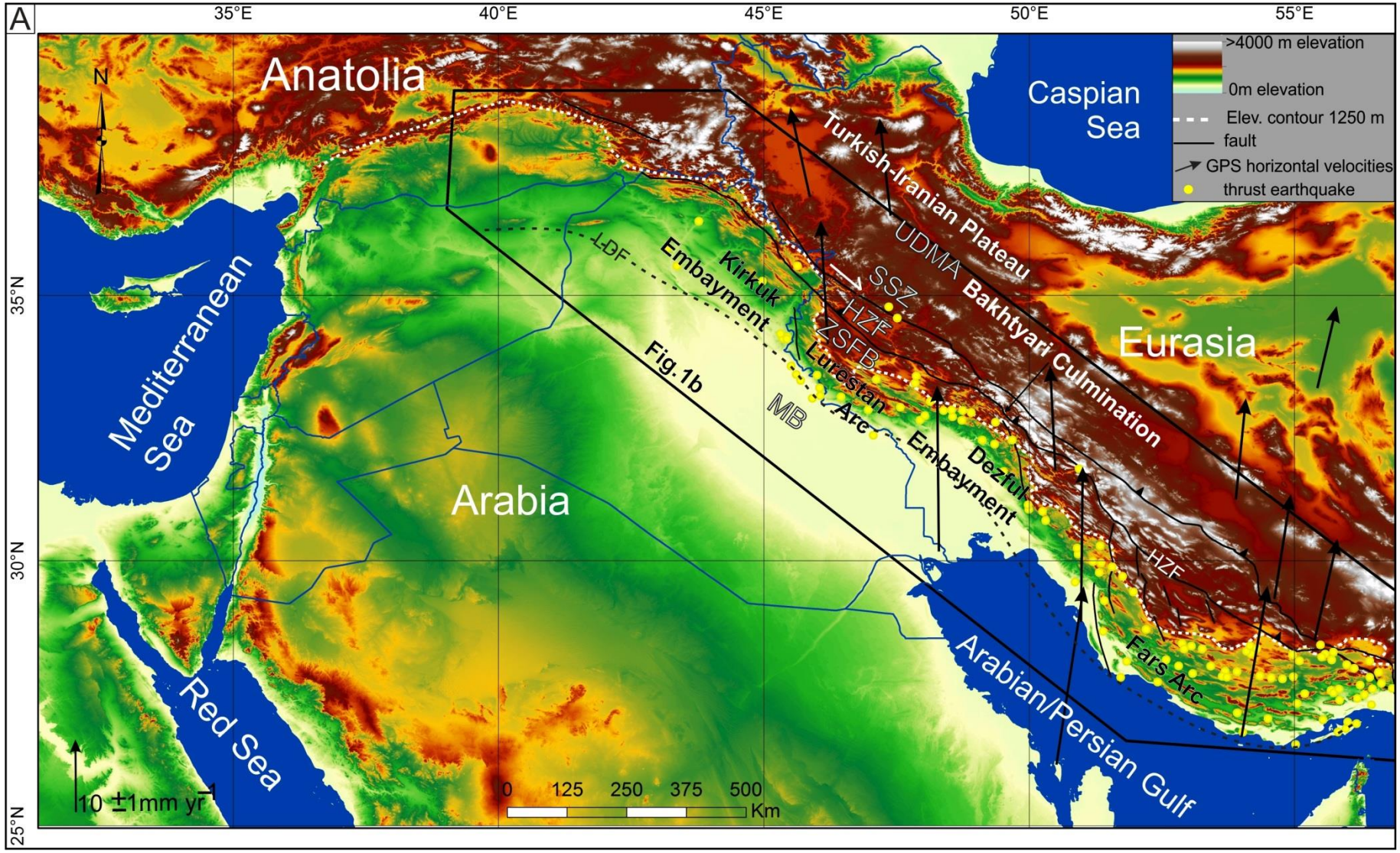
A
35°E
40°E
45°E
50°E
55°E
35°N
30°N
25°N
N
Anatolia
Caspian Sea
>4000 m elevation
0m elevation
Elev. contour 1250 m
fault
GPS horizontal velocities
thrust earthquake
Turkish-Iranian Plateau
UDMA
Bakhtyari Culmination
Eurasia
LDF
Embayment
Kirkuk
SSZ
HZF
ZSFB
Lurestan Arc
Fig.1b
MB
Dezful Embayment
Mediterranean Sea
Arabia
HZF
Red Sea
Arabian/Persian Gulf
Fars Arc
10 ±1mm yr⁻¹
0 125 250 375 500
Km

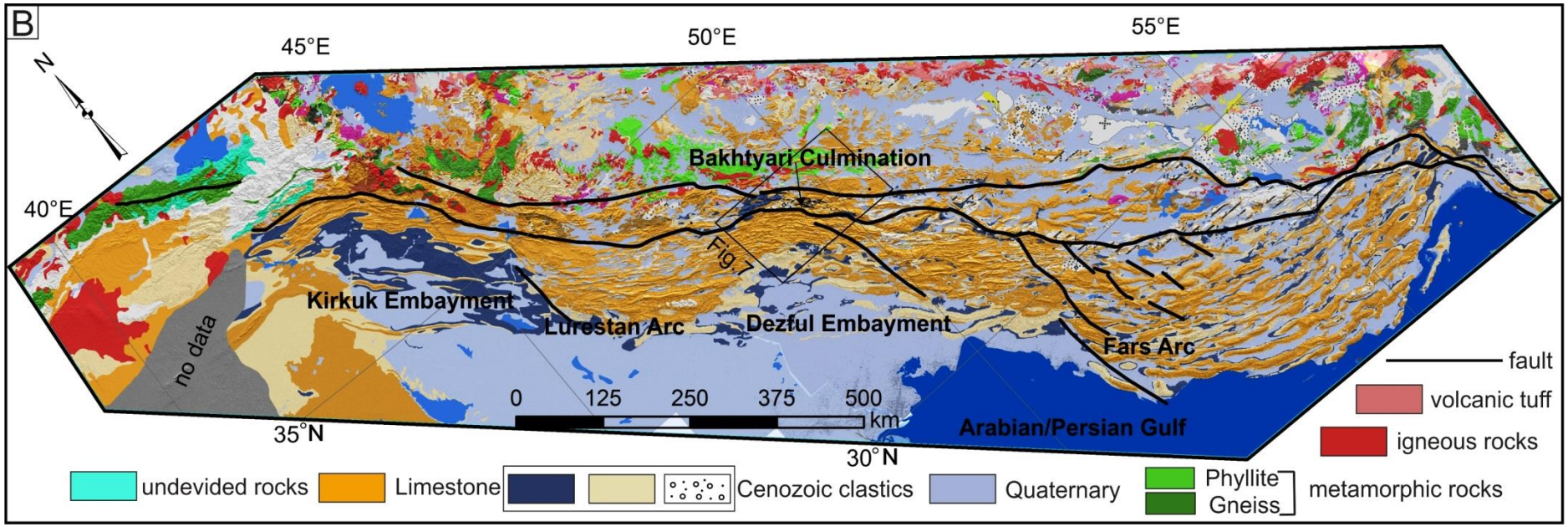

Fig.1. Regional topography, tectonics and lithologies of the Zagros fold-and-thrust belt. (a) Tectonic division zones after Berberian (1995), GPS velocities (stable Eurasia reference frame) after Vernant et al., 2004. UDMA = Urumieh-Dokhtar Magmatic Arc; SSZ = Sanandaj-Sirjan Zone; HZF = High Zagros Folds; ZSFB = Zagros Simply Fold Belt; LDF = Limit of Deformation Front; MB = Mesopotamian Basin. (b). Exposed lithologies of the Zagros fold-and-thrust belt (redrawn after (1) the geological map of Turkey 1:2,000,000; (2) Sissakian, 2000 and (3) Afaghi and Salek, 1975a; 1975b; 1977a; 1977b; 1977c; Afaghi et al., 1978).

1.1. Regional Zagros geology

The Zagros region has been subjected to a series of compressional and extensional phases during its geological history that have initiated and later reactivated a series of basement faults (Ameen 1992; Jassim and Goff 2006; Stern and Johnson 2010; Lacombe et al., 2011; Burberry 2015). The Arabia-Eurasia collision is only the latest of these events. The Zagros fold-and-thrust belt is built over what was the northern, passive continental margin of the Arabian Plate before its initial collision with Eurasia. Initial collision may have been roughly at the Eocene-Oligocene boundary (~35 Ma, Allen and Armstrong 2008; Perotti et al., 2016) or in the Late Oligocene-Early Miocene (~27-23 Ma, Mouthereau et al., 2012; McQuarrie and van Hinsbergen, 2013). The present Zagros fold-and–thrust belt (Fig. 1a) passes through the north and northeast of Iraq, across southern Iran and ends at ~57^{o} E where it juxtaposes the Makran accretionary complex (Mouthereau et al., 2006; Alavi 2007). GPS data suggests that the region accommodates a northward movement of the Arabian Plate at a rate of ~16-26 mm/yr (Vernant et al. 2004), with the convergence rate increasing eastwards.

The Zagros orogen consists of three main parallel tectonic units (Fig. 1a). From the northeast to the southwest these units are the subduction-related Urumieh-Dokhtar Magmatic Arc, the Sanandaj-Sirjan Zone and the Zagros fold-and-thrust belt.

Many folds have developed as a consequence of the Arabia-Eurasia collision. These are the classic “whaleback” structures of the Zagros fold-and-thrust belt, which trend NW-SE along the greater part of the range. Anticlines in the north western part of the Zagros (north of ~36^{o} N) and in the Fars region in the SE have more E-W trends (Fig.1). The High Zagros Fault separates the High Zagros folds to the north from the Simply Folded Belt to the south. Other structural divisions have been described across the strike of the orogen, but these are secondary, and bounded by features such as the Mountain Front Fault that may not be continuous along the length of the range (Fig.1).

Along the strike of the Zagros there are variations in the degree of exhumation, topographic elevation, relief, stratigraphy, position of the deformation front and structural style changes along strike (Talbot and Alavi, 1996). These along-strike changes divide the range into several domains, referred to as salients and embayments, adjacent to the higher elevation Turkish-Iranian Plateau to the northeast (Fig.1). These domains are the Kirkuk Embayment, Lurestan (Pusht-e Kuh) Arc, Dezful Embayment and Fars Arc, from the northwest to southeast (Berberian 1995; Lacombe et al., 2006; Mouthereau et al., 2007; Casciello et al.,

2009). The southwestern margins of the Kirkuk and Dezful embayments form a roughly linear deformation front, separated by the Lurestan/Pusht-e Kuh Arc (salient). To the southeast, the Fars Arc forms a curved deformation front, convex to the south. There are differences in the strain distribution within the Zagros related to the occurrence of the embayments (e.g. low strain in the Dezful Embayment complemented by high strain in Bakhtyari Culmination) (McQuarrie, 2004; Allen and Talebian, 2011). The origin of the Dezful Embayment has been related to the pre-continental collision of the Arabian Plate margin, and the irregular distribution of Cretaceous ophiolites upon it (Allen and Talebian 2011). It is not clear whether this model applies to the Kirkuk Embayment, however.

The boundary between the Simply Folded Belt and the Mesopotamian Foreland Zone is the current Zagros deformation front, although subtle Cretaceous-Cenozoic structures appear to the south of this line (including oil and gas fields). The pre-collisional significance of the boundary is unclear, but likely relates to differences in the Palaeozoic-Mesozoic rifting history of the Arabian Plate, associated with the opening of Tethys. The "Unstable" and "Stable" terms in stratigraphic descriptions (e.g. Jassim and Goff, 2006) relate to the differences began in the pre-Cenozoic, pre-collisional, history and stratigraphy.

Because the Zagros fold-and-thrust belt is built on the original passive continental margin of the Arabian Plate, the great majority of exposed rocks are sedimentary, and belong either to pre- or post-collisional sequences. Total sedimentary thickness commonly exceeds 10 km. Palaeozoic strata are rarely exposed. Precambrian basement occurs as fragments brought up by diapirs of the Hormuz Series salt, itself of latest Precambrian-Cambrian age. Carbonates occur at various levels within the stratigraphy, with important units in the Cretaceous (Bangestan Group) and mid Tertiary (Asmari Limestone and equivalents). Later Tertiary and Quaternary units are predominantly clastic, generally coarsen upwards and reveal the foreland propagation of deformation (Ruh et al., 2014). In terms of erodibility (Moosdorf et al., 2018), the carbonate units are particularly resistant, and commonly preserve the morphology of anticlines. Later Cenozoic clastic units are less resistant, and are more commonly preserved in synclines that are topographic lows between the anticlines. Within the Late Cenozoic clastics there are evaporites within the Gachsaran Formation and marl in the Mishan and Aghajari formations.

The climate of the Zagros is classified as arid to semi-arid with hot dry summers and cold dry winters (Kottek et al., 2006). The interaction between the Mediterranean and Sudan Lows

synoptic systems with different elevations across the Zagros Mountains produces precipitation variability in space and time (Boroujerdy et al., 2013).

2. Methods and data

2.1. Climate

Rainfall data from the Tropical Rainfall Measuring Mission satellite TRMM 3B43 (https://mirador.gsfc.nasa.gov/) were analysed for the time series 1998-2016 (resolution 0.25˚* 0.25˚~25*25 km) to allow investigation of first order precipitation variations on geomorphic indices (Section 3.1), and broader interactions with tectonics.

2. 2. Topographic swath profiles

Swath profiles represent continuous changes of surface altitude along the swath by maximum, mean and minimum elevations across the swath width. The general pattern of a landscape can be represented by the mean elevation. The difference between the maximum and the minimum elevations is the relief (Molin et al., 2004; Scotti et al., 2014) (also called incision by Andreani et al., 2014; although there is no requirement that a previous surface is incised).

Twenty-five swath profiles oriented NE-SW have been analysed (supplementary figure 1), using the Shuttle Radar Topography Mission (SRTM) 30 dataset (https://www2.jpl.nasa.gov/srtm/) (30 m pixel size). The width of swaths is 25 km on either side of the swath centre. Across-profile relief values were integrated to give an indication of overall relief for the range within each profile area. This is the first time this relief integration approach has been applied to the regional tectonic geomorphology of a fold-and-thrust belt, as far as we are aware. Therefore the Zagros system is something of a test case. The intention is to see what variation there is along the strike of the range, bearing in mind differences in the structure and climate, as well as any other potential variables.

2.3. Normalized river-channel steepness (k_{sn}) analysis

Features of active deformation can be recognised using the sensitivity of river profiles to uplift processes (Seeber and Gornitz, 1983). Tectonic geomorphology methods include the analysis of steady state river long profiles (e.g., Kirby et al., 2003; Snyder et al., 2000; Whipple and Tucker, 1999; Wohl and Merritt, 2001) or methods which recognise a change in base level (e.g., Boulton and Whittaker, 2009; Whipple, 2004; Whipple and Tucker, 1999,

2002; Whittaker and Boulton, 2012; Whittaker et al., 2007, 2008). Changes in the slope of river profiles can be recognized by the occurrence of knickpoints, both in slope-area or elevation-distance plots. Knickpoints can develop in response to tectonic effects (i.e. uplift caused by folding and/or faulting), or changes in base level (Goldrick and Bishop, 2007; Kirby and Whipple, 2012; Wobus et al., 2006), among other causes. Knickpoint distribution has been used to identify tectonic forcing in active orogens (Miller et al., 2012; Schildgen et al., 2012; Morell et al., 2012; Olivetti et al., 2012).

Tucker and Whipple (2002) and Whipple and Tucker (2002) described fluvial erosion in three conditions. These conditions are 1) detachment-limited models, which represent bedrock rivers where erosion is equal to uplift, and where a fall in base level or regional uplift and substrate erodibility control the gradient of river. 2) Transport-limited models, where channel gradient is determined by the capability of a river to transfer sediment. These cases are alluvial rivers. 3) The third case is hybrid river models, where substrate erodibility and sediment flux control the gradient of a channel. A dynamic equilibrium is required between two competitive parameters; the rate of rock uplift and the rate of terrain removal to preserve tectonic signals in the landforms (Dietrich et al., 2003).

The relationship between local slope of river channel (S) and upstream area (A) in the form of a power law (Hack's law) (Hack, 1957; Flint, 1974).

$$S = k_s A^{-\theta} \quad (1)$$

Where k_s and θ are the steepness index and concavity index, respectively. Slope-area plots allow the extraction of both S and A directly from DEMs using the regression of slope and area data. Accordingly, the concavity index, θ, and the steepness index, *k*s, can be calculated. The concavity index (θ) in Eq. (1) describes the change in slope along a graded river profile (Wobus et al., 2006). Significant deviation from a theoretical graded profile, with a smooth concave-up shape, reflects transient response to changes in tectonic rates (Boulton and Whittaker, 2009; Snyder et al., 2000; Larue, 2008), rock structures and their resistance differences (Larue, 2008; Phillips and Lutz, 2008) or other changes in base level and landscape (Bowman et al., 2007; Harmar and Clifford, 2007). Although the concavity index shows significant variability in natural streams, in a steady state it often has a value within the range ~0.4-0.6 (Kirby and Whipple, 2001; Snyder et al., 2000; Whipple, 2004; Wobus et al., 2006). A steady state condition means that there is a balance between erosion and surface

uplift. This uniformity leads to the insensitivity of the concavity index to the factors mentioned above. In contrast, the steepness index exhibits changes in value along the segmented profile, dependent on these factors. The steepness index incorporates the change in channel slope and drainage area, to deal with systematic variations in river gradient index as a result of changes in basin shape and discharge (Goldrick and Bishop, 2007).

To overcome the dependence of longitudinal profiles on the basin shape, a linear regression of gradient against drainage area should be applied on a log slope-log area plot. However, wide variation in k_s (regression intercept) can be the corollary of a small variation in θ (regression slope). So, relying on the assumption of a restricted range of the concavity index in a steady state ($0.4 \leq \theta \leq 0.6$) (Kirby and Whipple, 2001; Kirby and Whipple, 2012; Snyder et al., 2000; Wobus et al., 2003; Wobus et al., 2006), the normalized steepness index (k_{sn}) can be determined by evaluating slope-area regression using a reference concavity ($\theta_{ref} = 0.45$) in Eq. (2).

$$S = k_{sn} A^{-\theta ref} \quad (2)$$

Here, the variation in drainage area can be surmounted and effective comparison between streams profiles can be achieved, regardless of their catchment areas. In equilibrium landscapes, similar concavities for multiple segments of a stream profile can be recognised, but not similar steepness. Uplift results in steepened rivers, and accordingly the steepness index will vary (Dietrich et al., 2003; Snyder et al., 2000). Thus, k_{sn} can be used as a suitable metric in tectonic geomorphology studies (Kirby and Whipple, 2001; Wobus et al., 2006).

The SRTM 30 dataset (30 m pixel size) was used for the purpose of drainage network extraction, using MATLAB-based TecDEM 2.2 software (Shahzad and Gloaguen, 2011). The D8 algorithm (Jones, 2002) was applied to calculate flow directions.

The first step in deriving k_{sn} values is river profile generation. For this process, a minimum threshold of 10^5 m^2 contributing area was used to ensure fluvial dominated channel flow (Kirby and Whipple, 2001; Montgomery and Foufoula-Georgiou, 1994; Wobus et al., 2006). Using Stream Profiler software, the k_{sn} value was calculated for the whole Zagros using a reference concavity of $\theta_{ref} = 0.45$ (Wobus et al., 2006) to overcome lithological effects on the concavity index, and consequently the steepness index. Also we used TopoToolbox 2 MATLAB-based software (Schwanghart and Scherler, 2014) to calculate the k_{sn} of all river segments across the Zagros which have length more than 1 km. Results were compared with

lithologies represented on geological maps, to determine whether HI values are affected by active tectonic or lithological changes.

SRTM data have inherent errors (Boulton and Stokes, 2018) which result in voids that affect the flow-routing algorithm. Therefore, to test the method of river profile extraction, the QaraChwalan River profile was extracted manually from the SRTM 30 m data using Global Mapper GIS, and compared with the automatic extracted profile (supplementary Fig. 2). No difference was found between the two profiles, which indicates the reliability of the automatic drainage network extraction technique.

2.4. Hypsometric Index (HI)

The idea of hypsometry was first used to express the forms of drainage basins (catchments) and their slopes (Langbein, 1947). Strahler (1952) introduced the idea of the hypsometric index, or integral (HI).

For a given drainage basin, HI refers to the amount of residual terrain above the lowest horizontal plane of a basin and it can be used as a proxy for the erosional stage and landform development (Strahler, 1952; Schumm, 1956). High HI values (close to 1) mean that uplift is greater than erosion and the land surface is in a youthful stage, while low HI values (close to 0), erosion is greater than uplift and the land surface is in a mature stage. This dimensionless form enables the comparison between different basins regardless of their areas.

HI is a powerful tool to investigate the relative tectonism of an area, by characterizing the topographic dissection of a basin (Keller and Pinter, 2002). Due to the development of Digital Elevation Models (DEMs), HI can be calculated using Eq. (3) (Pike and Wilson, 1971; Keller and Pinter, 2002).

$$HI = \frac{H_{mean} - H_{min}}{H_{max} - H_{min}} \quad (3)$$

Where H_{max}, H_{min}, and H_{mean} are the maximum, minimum, and mean elevations respectively. We adopt the approach of Gao et al. (2016), who measured HI for drainage basins of a particular stream order to map out regional variations in the east of the Tibetan Plateau. The rationale is that drainage basins are naturally-defined areas that reflect both tectonics and lithology, and so align with changes in one or both of these parameters (e.g. slip and uplift on active faults).

The parameters of Eq. (3) were obtained directly from DEM data and HI was calculated using TecDEM 2.2 MATLAB-based and standard ArcGIS 10.3.1 software. The HI data were converted into raster mode using the polygon to raster function within the ArcGIS 10.3.1 to extract swath profiles for the HI data across different regions in the Zagros.

HI values for 4^{th} order (supplementary Fig. 3a) 5^{th} order (supplementary Fig. 3b) and 6^{th} order river basins (supplementary Fig. 3c) have been tested for a comparative analysis of HI values at different scales of drainage (supplementary Fig. 3a, b and c). The distribution of HI classes across the Zagros is similar for all orders of river basins, but the large area basins (i.e. 6^{th} order) lack enough resolution to distinguish changes in HI values and hence potential changes in tectonic style. Thus, the use of the third order river basin is preferred as it gives more detailed results about landscape response to tectonics. Using second or first order basins introduced problems because of the extra processing time required, and artefacts introduced by the resolution of the DEM data and the ability of the software to define drainage basins accurately.

3. Results

3.1. Climate

The TRMM 3B43 data show high variability in precipitation across different regions of the Zagros (Fig. 2), taking average annual values from the dataset. The maximum precipitation (~ 0.35 m/year) occurs in the Bakhtyari Culmination, parts of Lurestan and the northeast of the Kirkuk Embayment. The minimum precipitation (0.05 m/year) occurs in the central and eastern Fars regions, the interior of the Turkish-Iranian Plateau and in the foreland. In the Discussion we look at the geomorphic and tectonic data in the light of this climatic variation.

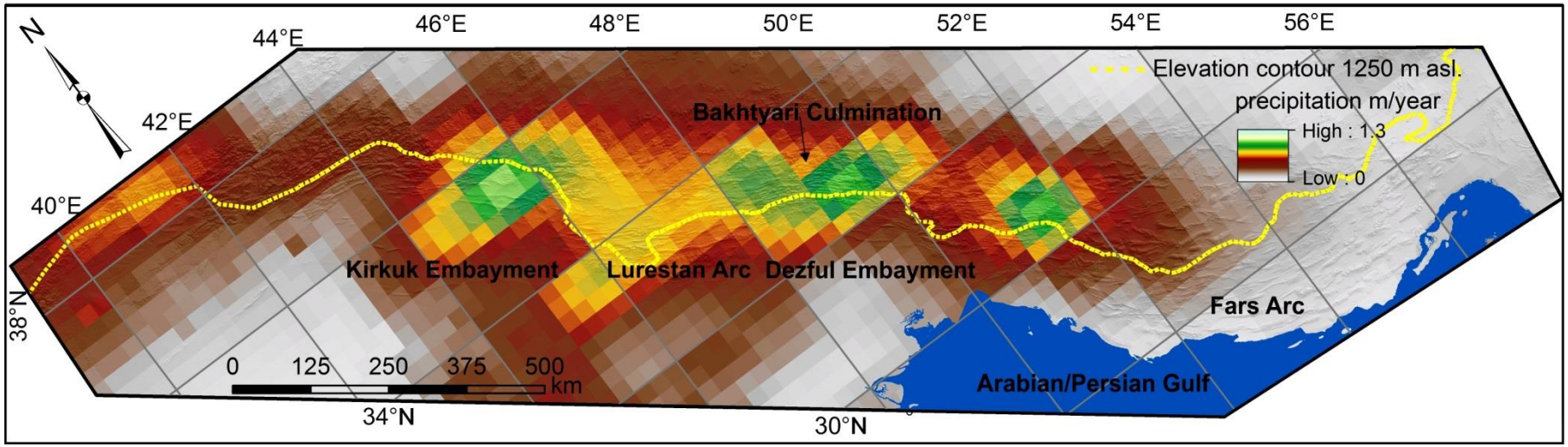

Fig. 2. SRTM 30 m shaded relief map of the Zagros, overlain by mean annual precipitation from the TRMM satellite (https://mirador.gsfc.nasa.gov/) for the period 1998-2016. Note the difference in precipitation between the Fars and Dezful/Bakhtyari regions.

3.2. Topographic swath profile analysis

Five swath profiles across the Zagros are shown in Fig. 3 as representative of the 25 analysed. These profiles show variations in topography across different regions of the range. The difference in elevation (relief) varies from ~<50 m within the Dezful Embayment to >2500 m in the Bakhtyari Culmination. Some profiles exhibit a gradual decline in elevation towards the foreland such as the Sinjar and Kirkuk profiles. Other profiles show a sharp drop towards the foreland, such as the Lurestan and Dezful examples. There is an increase in elevation and gradient towards the hinterland at or near the limit of seismogenic thrusting at 1250 m elevation (Allen et al., 2013) in both the Lurestan and Dezful sections. In contrast, there are very gentle changes in elevation across the Fars region, even when passing through the thrust seismicity cut-off at ~1250 m elevation, and across the High Zagros Fault. The difference between the maximum and the minimum elevations within the swaths (relief) shows where river networks dissect the landscapes. We integrate the relief of swath profiles (Fig. 3b). The cumulative difference between the maximum and minimum elevations (shaded areas in Fig. 3b) shows a difference of ~25% between the five profiles.

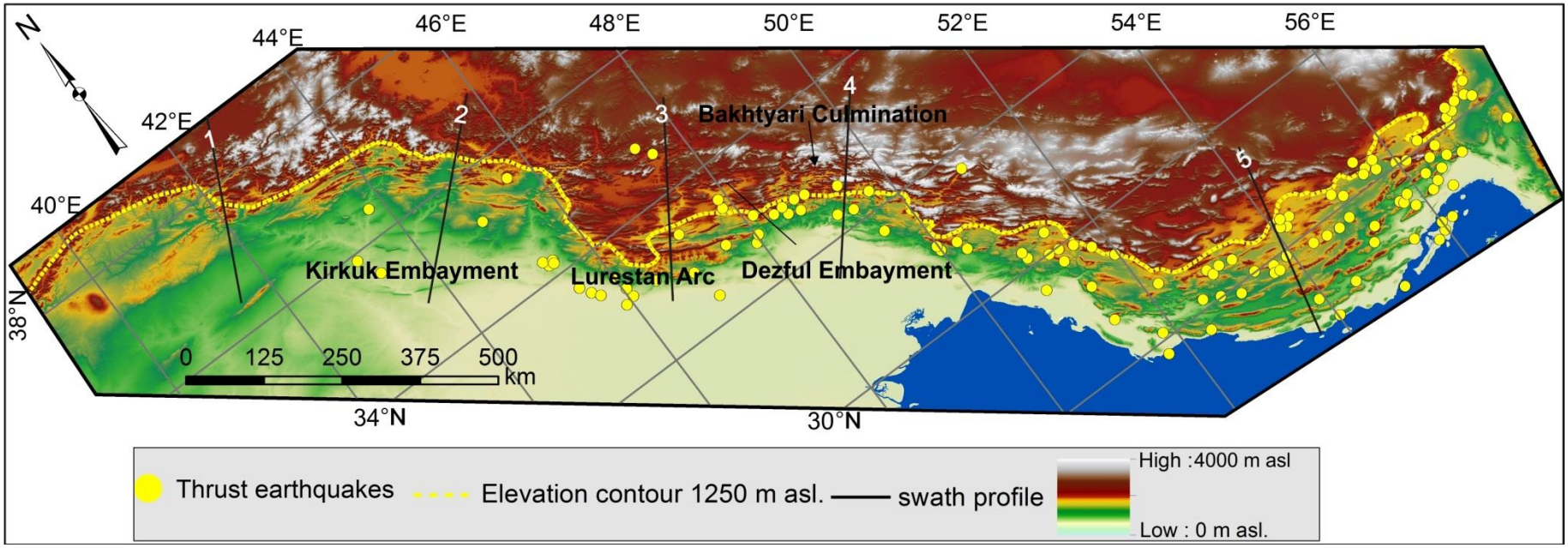
N
44°E
46°E
48°E
50°E
52°E
54°E
56°E
42°E
40°E
38°N
34°N
30°N
1
2
3
4
5
Bakhtyari Culmination
Kirkuk Embayment
Lurestan Arc
Dezful Embayment
0 125 250 375 500
km
Thrust earthquakes
Elevation contour 1250 m asl.
swath profile
High :4000 m asl
Low : 0 m asl.

306

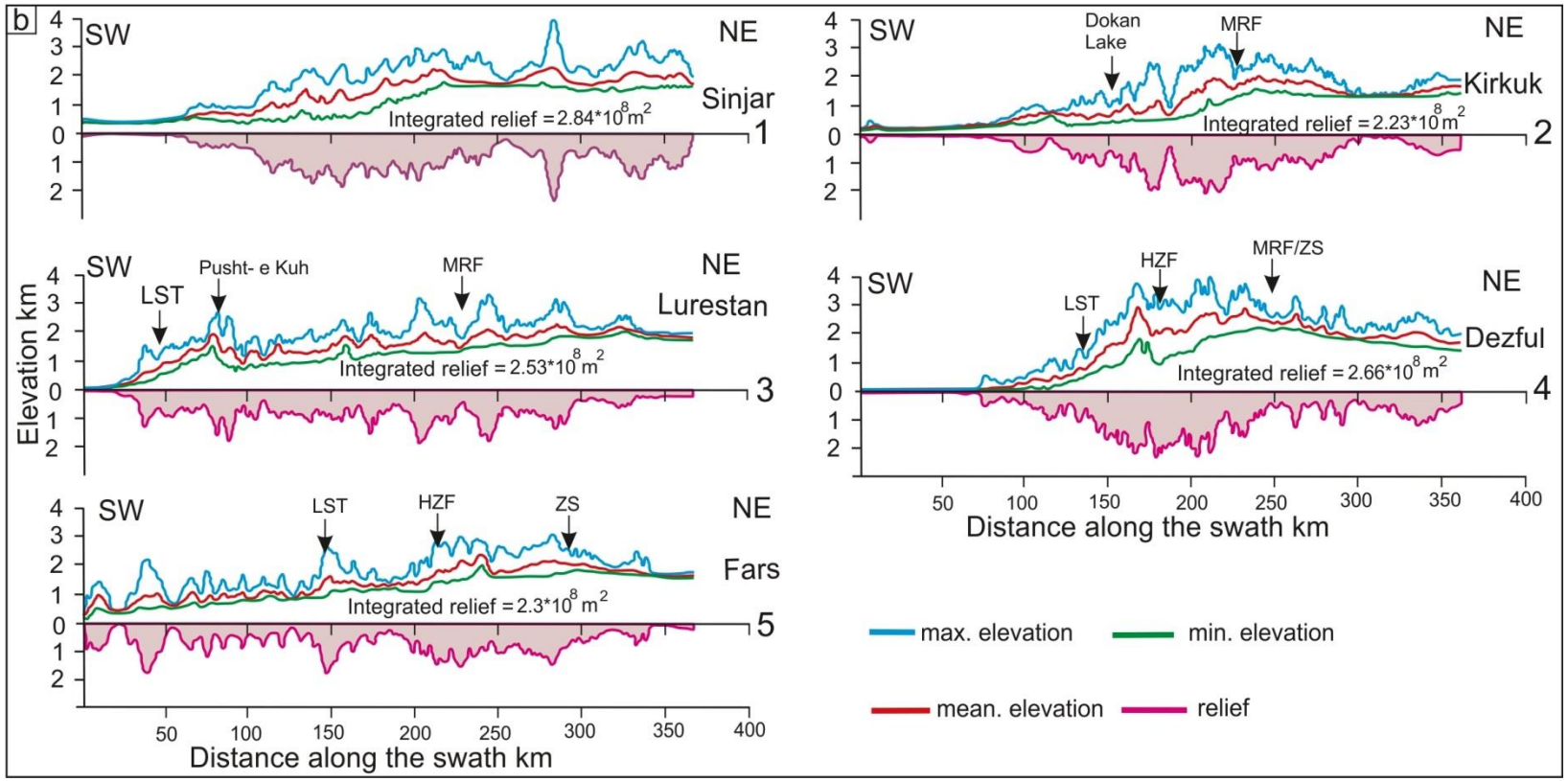

Fig. 3. SRTM 30 m topography of the Zagros fold-and-thrust belt. (a) Locations for topographic swath profiles. (b) Mean, Maximum and minimum elevation along the swath profiles. Integrated relief graphs show a limited relief difference in the order of ~25% between representative swath profiles. LST = Limit of seismogenic thrusting; HZF = High Zagros Fault; MRF = Main Recent Fault; ZS = Zagros Suture.

3.3. Normalized river-channel steepness (k_{sn})

Longitudinal profiles (supplementary figure 4) were generated for all river segments with a length of more than 1 km (Fig. 4a and b). Reaches of k_{sn} <50 $m^{0.9}$ are distributed across the Iranian plateau, the foreland, intermontane rivers and the Fars region (Fig. 4). Ranges of 50 ≤ k_{sn} ≤100 $m^{0.9}$ occur in the high relief areas of the Bakhtyari Culmination, Sirwan River basin, and in terrain at close the 1250 m elevation contour in the NW Zagros, near the Iraq-Turkey border (Fig. 4). A similar distribution occurs across the high relief areas when considering the range of 100 ≤ k_{sn} ≤150 $m^{0.9}$ (Fig. 4). Values of k_{sn} ≥150 $m^{0.9}$ occur only for a few river segments in the high relief areas of the Bakhtyari and the NW Zagros of Iraq and Turkey (Fig.4). Generally, the Fars region exhibits relatively low k_{sn} values compared with other areas of the Zagros (Fig. 4).

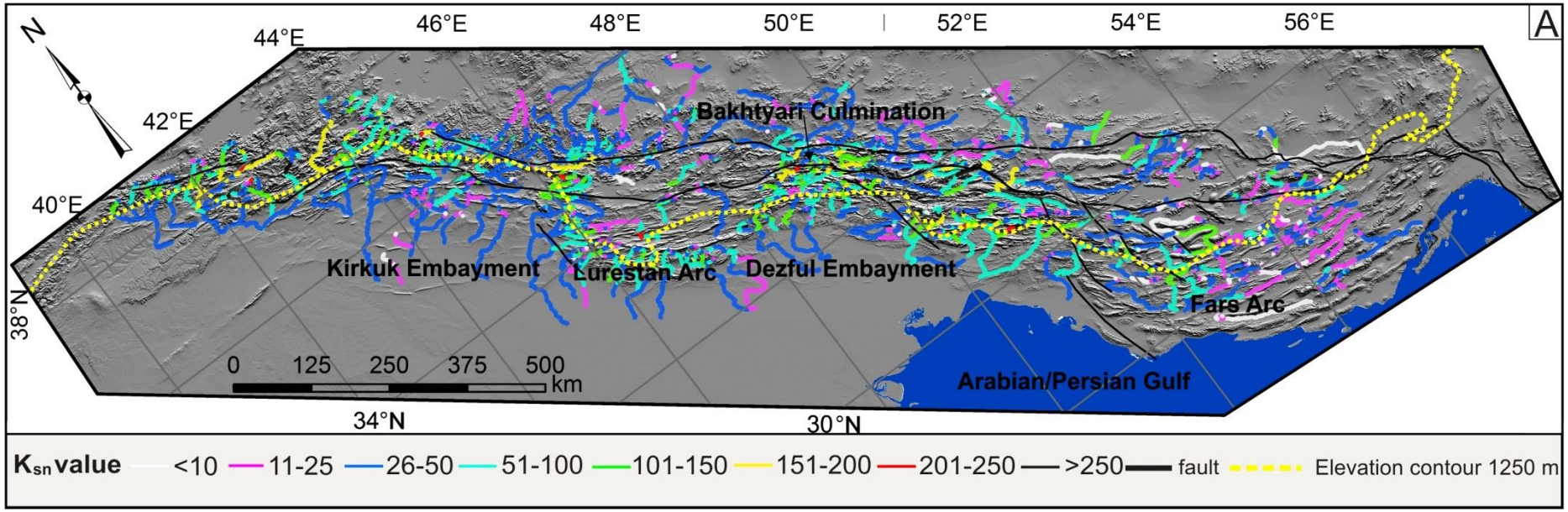
A
N
44°E
46°E
48°E
50°E
52°E
54°E
56°E
42°E
40°E
38°N
34°N
30°N
Bakhtyari Culmination
Kirkuk Embayment
Lurestan Arc
Dezful Embayment
Fars Arc
Arabian/Persian Gulf
0 125 250 375 500
km
Ksn value
<10
11-25
26-50
51-100
101-150
151-200
201-250
>250
fault
Elevation contour 1250 m

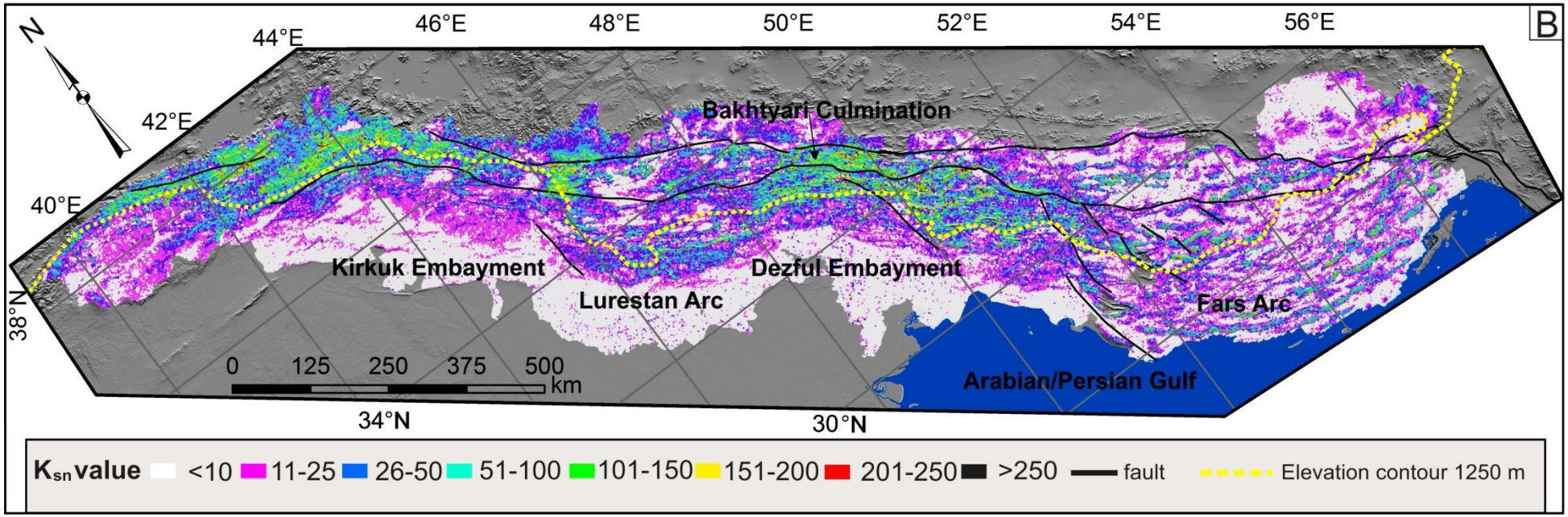

Fig.4. Distribution of k_{sn} values for Zagros river segments. (a) k_{sn} values using MATLAB-Based stream profiler; note the low values in the Fars region. (b) k_{sn} values extracted using TopoToolbox software. Note the high values in the Bakhtyari Culmination and the northeast of the Kirkuk Embayment.

3.4. Hypsometric Index (HI)

Results from 17380 third order river basins across the Zagros reflect two major groups of relative low HI values (HI <0.3) (Fig. 5). The first group of relative low HI values represents the Turkish-Iranian Plateau where topographic gradients are very low (Allen et al., 2013). The second group of relative low HI region occurs across the foreland and Mesopotamian plain. Intermediate and relatively high HI values (>0.3) occur across the mountainous areas of the Zagros which are characterized by high relief and gradient (Fig. 6). Highest values occur northeast of the Kirkuk Embayment, in the Bakhtyari Culmination, and close to the coast in the Fars region (Fig. 5).

Along much of the Zagros there is a coincidence between the transition limit from HI values of <0.3 to >0.3 upper elevation limit of seismogenic thrusting (Fig. 5). This pattern is seen northeast of the Kirkuk Embayment, along the Lurestan/Pusht-e Kuh Arc and in the region of the Kazerun Fault (western Fars). Different patterns occur in the Bakhtyari Culmination and in the southeast of the Zagros (Fars region). In the Bakhtyari Culmination relatively high HI values persist northeast of (above) the 1250 m elevation contour and the limit of seismogenic thrusting. In the Fars region, seismogenic thrusting continues north of the transition from high to low HI values (taken as HI = 0.3).

Swath profiles from raster data of the HI value across the Zagros (Fig. 6) show the HI value increasing in areas of high relief but not within high elevation regions. Differences in lithology have been examined to assess whether lithology is a significant control on HI value: Figure 7 shows both HI values and lithologies for the Bakhtyari Culmination; there is no clear correlation between them.

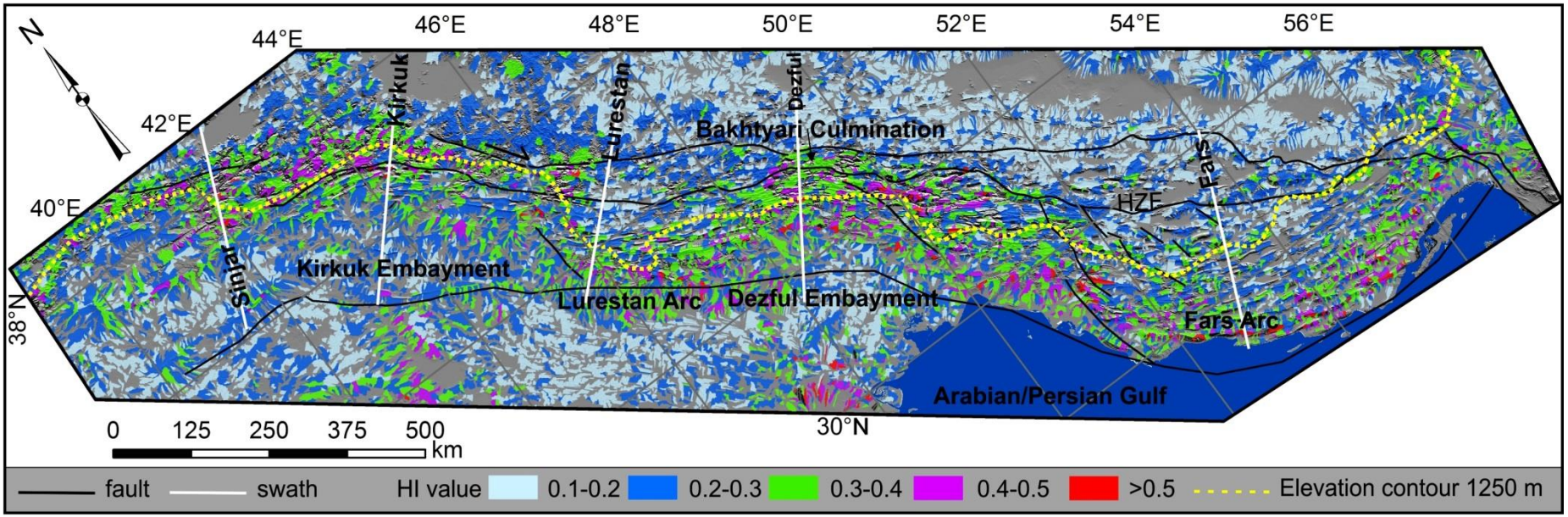

Fig. 5. HI values for 3rd order drainage basins across the Zagros. There is a broad region of relative high HI (>0.3; green-amethyst colours) along the Zagros, between the Iranian Plateau and the foreland. Specific regions show variations to this broad trend. In the Bakhtyari Culmination, the high/low HI transition lies at higher elevations than the thrust seismicity cut-off (~1250 m elevation contour), while in the Fars region the high/low HI transition takes place at lower elevations than this cut-off.

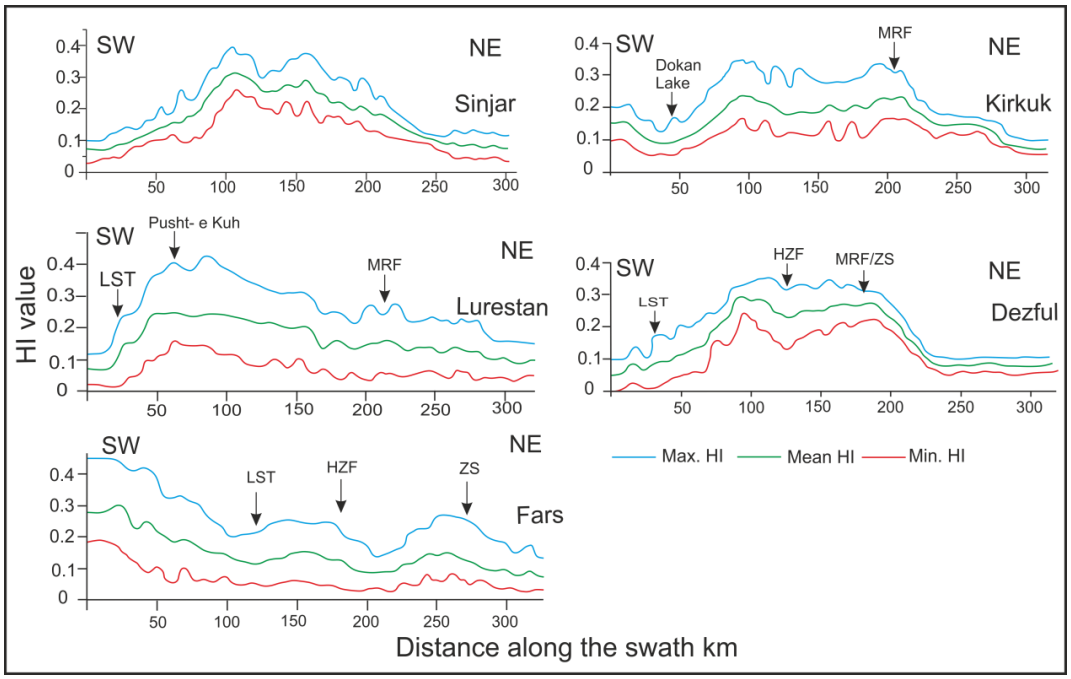

Fig.6. Swath profiles extracted from HI raster data show the variation in HI across the Zagros range along the swaths in Fig. 5. The width of swaths is 25 km on either side of the swath centre. LST = Limit of seismogenic thrusting; ZS = Zagros Suture; HZF = High Zagros Fault; MRF = Main Recent Fault. The Fars region has high HI values southwest of the LST, in the opposite sense to the Dezful region.

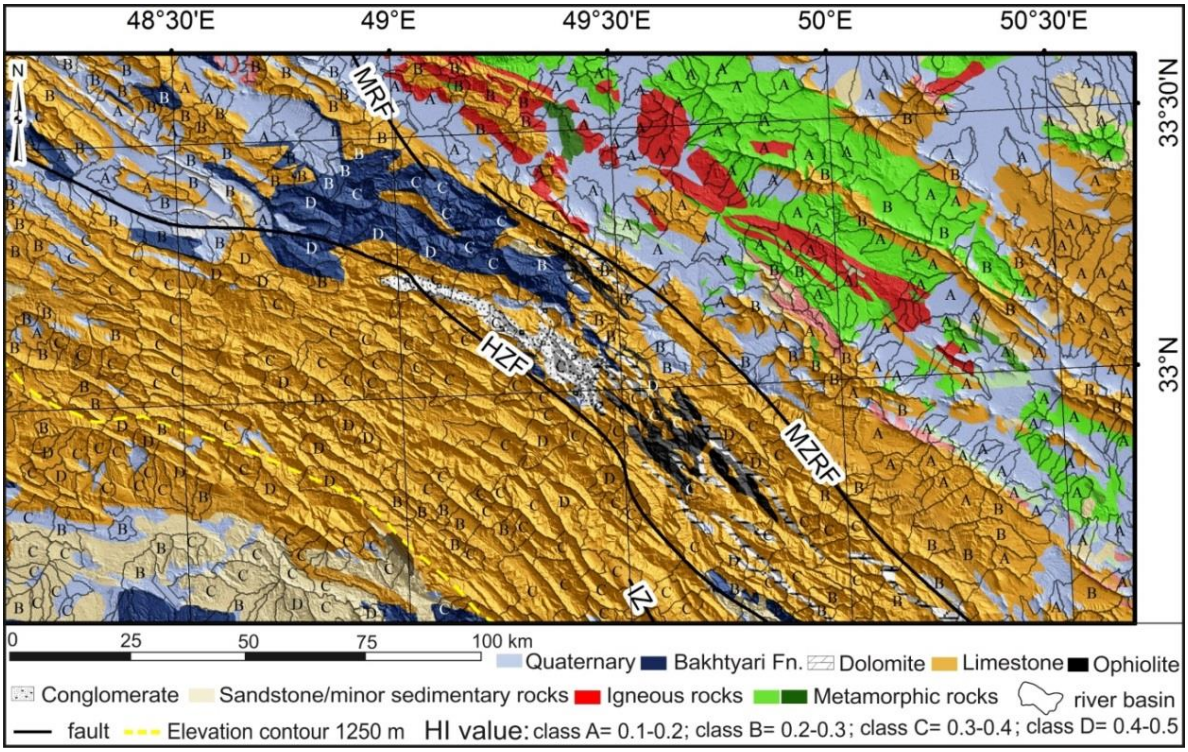

Fig. 7. HI values in the Bakhtyari Culmination plotted over the geological map (geology from sources in Fig. 1b), which shows similar HI values across different lithologies, and different HI values across the same lithology.

4. Discussion

4.1. Swath profiles

The Sinjar, Kirkuk and Fars sections show steady increases in elevation toward the hinterland for the first ~200 km of the swath profiles (Fig. 3), which is well-established by previous work (see McQuarrie, 2004; Mouthereau et al., 2012; Allen et al., 2013 and references therein). Integrating the relief along each profile (Fig. 3) shows the values for each profile are within ~25% of each other, at 2.2 – 2.8 x 10^8 m^2. Given that this is a new approach to analyzing the geomorphology of active fold-and-thrust belts, it is not possible to make detailed comparisons with other ranges. However, we suggest that a ~25% variation is not large, considering the variation is structure and climate in different parts of the Zagros. This in turn suggests that the integrated relief of the mountain range may be less controlled by the parameters which vary along the Zagros, such as the width of the seismogenic belt, or maximum topographic gradient, and more by parameters which are similar across strike, such as strain rate (Masson et al., 2005), overall shortening (McQuarrie, 2004; Vergés et al., 2011; Allen et al., 2013), or the elevation difference between the hinterland plateau and the undeformed foreland.

4.2. Normalized river-channel steepness (k_{sn})

Bearing in mind that surface uplift is extremely unlikely to be uniform across the entire Zagros, with implications for the applicability of a uniform approach to analyzing k_{sn} (Snyder et al., 2000), there are broad differences in k_{sn} values as follows. There is a general pattern that higher k_{sn} values occur where the rivers cross the 1250 m contour (Fig. 4), and so from the interior, relatively aseismic region into the thrust-seismogenic part of the Zagros, but this is a broad distinction, without a sharp change. k_{sn} values are lower in the Fars region than elsewhere in the Zagros. Kirby and Whipple (2012) noted the correlation between the linear physiographic transition of Lesser/Greater Himalaya and the northward increase in k_{sn} values. The zone of high k_{sn} values is on the hanging wall of the Himalayan Main Central Thrust (MCT), interpreted as relating to the active uplift in the vicinity of this fault. The Longmenshan in SE Tibet is another example of a sharp boundary between high and low k_{sn} values, in the region of the active Yingxiu-Beichuan and Pengguan faults (Gao et al., 2016).

Such sharp distinctions have not been found in the k_{sn} distribution of the Zagros, perhaps due to the tectonic difference between the multiple, segmented, blind thrusts of the Zagros, and the laterally continuous and large scale thrusts of the Himalaya (i.e. the MCT) and SE Tibet.

Rivers in the Fars region commonly divert around the tips of anticlines or cross relay zones between them. This is because of low discharge of rivers including the internally drained basins in the region. The relatively dry climate has led to limited and ephemeral discharge of rivers which is not enough to overcome the growth of anticlines. Therefore the Fars region rivers have low k_{sn} values (Fig. 4) and commonly divert around anticlines (Ramsey et al., 2008). Although there are many anticlines and active seismicity in the Fars region, the dry climate has an important effect in the formation of axial rivers (Ramsey et al., 2008). Transverse rivers commonly occur in the Dezful/Bakhtyari region as a result of relatively high precipitation and intense thrusting in the Bakhtyari Culmination, which enable rivers to incise as they cross numerous anticlines.

4.3. Hypsometric Index (HI)

In the Bakhtyari Culmination (Fig. 7) we examine changes in bedrock lithologies and their effects on the HI value. The Culmination consists mainly of limestones, limestones alternating with marls and conglomerates, patches of ophiolitic lithologies (e.g. serpentinite, basalt), and sandstones and conglomerates of the Bakhtyari Formation. To the northeast of the Culmination there is a series of igneous and metamorphic rocks. For the same lithology there are significant differences in the HI value. In contrast, there are areas where different lithologies, such as the ophiolitic assemblages and limestones, show similar HI values (0.3-0.4) (Fig. 7). This result implies that differences in lithology have limited effects on the HI value.

Figure 2 shows the climatic variation within and across the Zagros, with a seven-fold difference between annual precipitation in the wettest areas (Dezful/Bakhtyari Culmination) and the driest areas (parts of Fars). The relatively wet climate in the Dezful/Bakhtyari regions (Fig. 2) enables the river system to erode the landscape in an area where deformation takes place predominantly in a narrow zone of high strain (Allen et al., 2013) and steep slopes: the Bakhtyari Culmination. The high HI region continues to the northeast of the seismogenic limit of thrusting (Fig. 5). From the tectonic perspective, this region has become part of the Turkish-Iranian Plateau, in that it is not experiencing active (seismogenic) shortening; from a

geomorphic perspective, it has not yet become a relatively low relief plateau, because of the relief created and maintained by the drainage network (Figs. 5 and 6).

In the Fars region, the exposed lithology is mainly limestone, which resists erosion on the flanks and crests of anticlines (Fig. 1). The relatively dry climate in Fars (Fig. 2), combined with low regional gradients and sinuous rivers, reduces stream power, and thus erosion rates. Consequently, the low HI zone occurs south of the limit of seismogenic thrusting (Fig. 5). This part of the Fars region behaves in the opposite sense to the Dezful/Bakhtyari region, in that it still experiences thrust seismicity, even in a low relief area that resembles the essentially aseismic plateau interior further north (Fig. 8). We attribute the difference in the location of the low/high HI transition to differences in the basement of the Dezful/Bakhtyari and Fars regions. Deformation is focused in the Bakhtyari Culmination because the adjacent Dezful Embayment resists deformation, attributed by Allen and Talebian (2011) to the different pre-collisional histories of the Dezful Embayment and adjacent areas. There is no difference within the Fars region (Allen et al., 2013; Talebian and Jackson, 2004). These tectonic differences have a climatic positive feedback result in the relatively wet climate in the Dezful/Bakhtyari, where there is a higher topographic barrier, while in contrast, a relatively dry climate and low relief occur in the Fars region (Figs. 1, 2 and 5).

Regional analysis of HI values on a drainage basin scale does not show sharp changes across individual structures, which would be expected if active deformation was controlled by a small number of major thrusts in the Zagros. This pattern contrasts with the east of the Tibetan Plateau (Longmenshan), where such abrupt jumps in HI have been observed (Gao et al., 2016).

In the Zagros study area, HI is a more effective tool than k_{sn} analysis, for highlighting geomorphic variations that relate to the active tectonics and climate. We do not make this as a universal claim, but it will be interesting to apply HI analysis in the form used by Gao et al (2016) and in this paper, to other active fold-and-thrust belts in the world.

5. Conclusions

In this paper we show that the geomorphic index HI provides insights into the landscape response to tectonics and climate in the Zagros (Fig. 5), and it is more effective in this regard than the more commonly used k_{sn} analysis (Fig. 4). Differences in geomorphic indices across two specific areas in the Zagros can be explained by the different climate of the two areas:

458 wetter conditions and vigorous drainage systems in the Dezful/Bakhtyari region retard plateau
459 growth; drier climate leads to low stream power of rivers in the Fars region and promotes
460 plateau growth (Fig. 8). The cut-off in thrust seismicity, proxied by the 1250 m elevation
461 contour, provides a simple tectonic boundary marker for comparison (Nissen et al., 2011).
462 Orographic precipitation may itself have a tectonic control; regional basement strength
463 variations are another plausible cause (Allen and Talebian, 2011). Strong basement in the
464 Dezful Embayment keeps the amount of strain low in this region, but produces intense
465 thrusting and steep relief in the Bakhtyari Culmination to its northeast, so that the overall
466 strain across this part of the Zagros is similar to adjacent regions (Allen and Talebian, 2011).
467 It is possible that the Kirkuk Embayment has a similar origin to the Dezful Embayment, with
468 the same consequence, that high strain is concentrated in the imbricate zone to its northeast
469 where high k_{sn}, HI and high relief occur.

470 We conclude that there is a positive feedback of tectonics and climate, which leads to the
471 wetter climate in the Bakhtyari Culmination, and causes rivers to cut efficiently through
472 landscapes. Youthful, high relief landscapes are the result, in contrast with the drier climate of
473 the Fars region: the Fars climate promotes subdued landscapes and plateau-like
474 geomorphologies in an area that is actively shortening by seismogenic thrusting.

475 Integrated relief along five topographic swath profiles is similar to within ~25% (Fig. 3).
476 These profiles are different to each other in terms of the distribution of elevation and climate.
477 We argue that the degree of relative similarity between the integrated relief is related to one or
478 more of the parameters that are similar between different regions, such as such as strain rate,
479 overall shortening, or the elevation difference between the hinterland plateau and the
480 undeformed foreland.

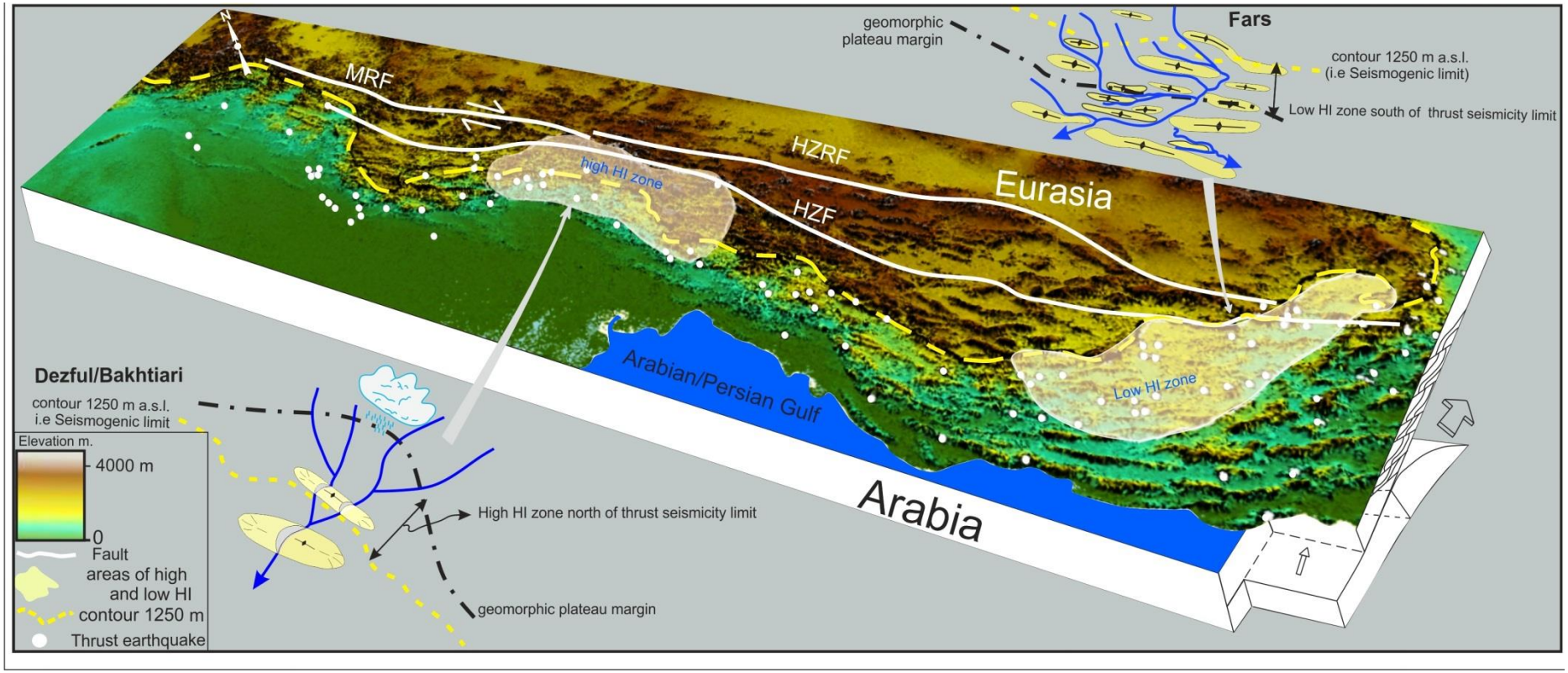

Fig. 8. Model showing how the Zagros topography responds to tectonism in term of changes in HI value. Relative high and relative low HI regions relate to the cut-off in thrust seismicity (proxied by the 1250 m elevation contour). The geomorphic plateau margin is retarded to the northeast in the Dezful/Bakhtyari region, and advances southwest in the Fars region.

Acknowledgements

We thank the Ministry of Higher Education and Scientific Research in Iraq for their support of the first author's project. We thank Chris Saville for useful discussion of geomorphic indices and Sarah Boulton for her help with stream profile analysis. The first author would like to thanks the Institution of Geological Survey of Iraq (GEOSURV) for providing geological maps included in this paper. Christoph Grützner and David Fernández-Blanco provided constructive reviews. We are grateful to Christoph von Hagke and Olivier Lacombe for handling the editorial process.

References

Afaghi, A, Salek, M. M., 1975a. Geological map of Iran, sheet No., 5 North-west Iran, National Iranian Oil Company, Tehran, Iran, scale 1:1,000,000.

Afaghi, A, Salek, M. M., 1975b. Geological map of Iran, sheet No., 4 South-West Iran, National Iranian Oil Company, Tehran, Iran, scale 1:1,000,000.

Afaghi, A, Salek, M. M., 1977a. Geological map of Iran, sheet No., 2 North-Central Iran, National Iranian Oil Company, Tehran, Iran, scale 1:1,000,000.

Afaghi, A, Salek, M. M., 1977b. Geological map of Iran, sheet No., 3 North-East Iran, National Iranian Oil Company, Tehran, Iran, scale 1:1,000,000.

Afaghi, A, Salek, M. M., 1977c. Geological map of Iran, sheet No., 6 South-East Iran, National Iranian Oil Company, Tehran, Iran, scale 1:1,000,000.

Afaghi, A, Salek, M. M., Moazami, J., 1978. Geological map of Iran, sheet No., 1 North-west Iran, National Iranian Oil Company, Tehran, Iran, scale 1:1,000,000.

Alavi, M., 2007. Structures of the Zagros fold-thrust belt in Iran. American Journal of Science 307, 1064–1095.

Allen, M. B., Armstrong, H. A., 2008. Arabia-Eurasia collision and the forcing of mid-Cenozoic global cooling. Palaeogeography, Palaeoclimatology, Palaeoecology. 265, 52–58.

Allen, M. B., Talebian, M., 2011. Structural variation along the Zagros and the nature of the Dezful Embayment. Geological Magazine 148, 911-924. doi:10.1017/S0016756811000318.

Allen, M. B., Saville, C., Blanc, E. J.-P., Talebian, M., Nissen, E., 2013. Orogenic plateau growth: Expansion of the Turkish-Iranian Plateau across the Zagros fold-and-thrust belt, Tectonics 32, 171–190, doi:10.1002/tect.20025.

518 Ameen, M. S., 1992. Effect of basement tectonics on hydrocarbon generation, migration, and
519 accumulation in Northern Iraq. American Association of Petroleum Geologists Bulletin
520 76, 356–370.

521 Andreani, L., Stanek, P. K., Gloaguen, R., Krentz, Ottomar, Dominquez-Gonzalez, L., 2014.
522 DEM-Based Analysis of interactions between tectonics and landscapes in the Or
523 Mountain and Eger Rift (East Germany and NW Czech Republic). Remote Sensing 6,
524 7971–8001.

525 Bahrami, S., 2013. Analyzing the drainage system anomaly of zagros basins: Implications for
526 active tectonics. Tectonophysics 608, 914–928.

527 Berberian, M., 1995. Master "blind" thrust faults hidden under the Zagros folds: active
528 basement tectonics and surface morphotectonics. Tectonophysics 241, 193–224.

529 Blanc, E. J.-P., Allen, M. B., Inger, S., Hassani, H., 2003. Structural styles in the Zagros
530 Simple Folded Zone, Iran. Journal of the Geological Society 160, 40–412.

531 Boroujerdy, P., Nasrollahi, N., Hsu, K., Sorooshian, S., 2013. Evaluation of satellite-based
532 precipitation estimation over Iran. Journal of Arid Environments 97, 205–219.

533 Boulton, S.J., Whittaker, A.C., 2009. Quantifying the slip rates, spatial distribution and
534 evolution of active normal faults from geomorphic analysis: Field examples from an
535 oblique-extensional graben, southern Turkey. Geomorphology 104, 299–316.

536 Boulton, S.J., Stokes, M., 2018. Which DEM is best for analyzing fluvial landscape
537 development in mountainous terrains? Geomorphology 310, 168-187.

538 Bowman, D., Shachnovich-Firtel, Y., Devora, S., 2007. Stream channel convexity induced by
539 continuous base level lowering, the Dead Sea, Israel. Geomorphology 92, 60–75.
540 doi:10.1016/j.geomorph.2007.02.009.

541 Bretis, B., Bartl, N., Grasemann, B., 2011. Lateral fold growth and linkage in the Zagros fold
542 and thrust belt (Kurdistan, NE Iraq). Basin Research 23, 615–630.

543 Burberry, C.M., Cosgrove, J.W. and Liu, J.G., 2008. Spatial arrangement of fold types in the
544 Zagros Simply Folded Belt, Iran, indicated by landform morphology and drainage
545 pattern characteristics. Journal of Maps 4, 417-430.

546 Burberry, C. M., Cosgrove, J. W. Liu, J.-G., 2010. A study of fold characteristics and
547 deformation style using the evolution of the land surface: Zagros Simply Folded Belt,
548 Iran. Geological Society, London, Special Publications 330,139-154.

549 Burberry, C. M. 2015. The effect of basement faults reactivation on the Triassic-Recent

550 geology of Kurdistan , North Iraq. Journal of Petroleum Geology 38, 37–58.
551 Casciello, E., Vergés, J., Saura, E., Casini, G., Fernandez, N., Blanc, E., Homke, S., Hunt,
552 D.W., 2009. Fold patterns and multilayer rheology of the Lurestan Province, Zagros
553 Simply Folded Belt (Iran). Journal of the Geological Society 166, 947–959.
554 Dietrich, W.E., Bellugi, D.G., Heimsath, A.M., Roering, J.J., Sklar, L.S., Stock, J.D., 2003.
555 Geomorphic Transport Laws for Predicting Landscape Form and Dynamics. Geophys.
556 Monogr. 135, 1–30. doi:10.1029/135GM09
557 Fakhari, M.D., Axen, G.J., Horton, B.K., Hassanzadeh, J., Amini, A., 2008. Revised age of
558 proximal deposits in the Zagros foreland basin and implication for Cenozoic evolution of
559 the High Zagros. Tectonophysics 451, 170–185.
560 Flint, J.J., 1974. Stream gradient as a function of order, magnitude, and discharge. Water
561 Resources Research 10, 969–973. doi:10.1029/WR010i005p00969.
562 Gao, M., Zeilinger, G., Xu, X., Tan, X., Wang, Q., Hao, M., 2016. Active tectonics evaluation
563 from geomorphic indices for the central and the southern Longmenshan range on the
564 Eastern Tibetan Plateau, China. Tectonics, 35, 1812–1826, doi:10.1002/2015TC004080.
565 Ghasemi, A., Talbot, C., 2006. A new tectonic scenario for the Sanandaj-Sirjan Zone (Iran).
566 Journal of Asian Earth Sciences 26, 683–693.
567 Goldrick, G., Bishop, P., 2007. Regional analysis of bedrock stream long profiles: evaluation
568 of Hack's SL form, and formulation and assessment of an alternative (the DS form).
569 Earth Surface Processes and Landforms 32, 649–6714. doi:10.1002/esp.
570 Hack, J.T., 1957. Studies of Longitudinal Stream Profiles in Virginia and Maryland. U.S.
571 Geological Survey Professional Paper 294-B, 97.
572 Harmar, O.P., Clifford, N.J., 2007. Geomorphological explanation of the long profile of the
573 Lower Mississippi River. Geomorphology 84, 222-240.
574 doi:10.1016/j.geomorph.2006.01.045.
575 Jassim, S. Z., Goff, J.C., 2006. Geology of Iraq, first ed. Dolin Prague and Moravian
576 Museum, Prague (341pp).
577 Jones, R., 2002. Algorithms for using a DEM for mapping catchment areas of stream
578 sediment samples. Computers and Geosciences 28, 1051-1060.
579 Keller, E., Pinter, N., 2002. Active Tectonics: Earthquakes, Uplift, and Landscape. Prentice
580 Hall, New Jersey.
581 Khadivi, S., Mouthereau, F., Larrasoaña, J.C., Vergés, J., Lacombe, O., Khademi, E.,
582 Beamud, E., Melinte-Dobrinescu, M. and Suc, J.P., 2010. Magnetochronology of
583 synorogenic Miocene foreland sediments in the Fars arc of the Zagros Folded Belt (SW

584 Iran). Basin Research 22,918-932.
585 Khadivi, S., Mouthereau, F., Barbarand, J., Adatte, T. and Lacombe, O., 2012. Constraints on
586 palaeodrainage evolution induced by uplift and exhumation on the southern flank of the
587 Zagros–Iranian Plateau. Journal of the Geological Society 169, 83-97.
588 Kirby, E., Whipple, K., 2001. Quantifying differential rock-uplift rates via stream profile
589 analysis. Geology 29, 415-418.
590 Kirby, E., Whipple, K.X., Tang, W., Chen, Z.,2003. Distribution of active rock uplift along
591 the eastern margin of the Tibetan plateau:inferences from bedrock river profiles. Journal
592 of Geophysical Research: Solid Earth 108, 2217.
593 http://dx.doi.org/10.1029/2001JB000861.
594 Kirby, E., Whipple, K.X., 2012. Expression of active tectonics in erosional landscapes. Journa
595 of Structural Geology 44, 54–75. doi:10.1016/j.jsg.2012.07.009.
596 Koshnaw, R.I., Horton, B.K., Stockli, D.F., Barber, D.E., Tamar-Agha, M.Y., Kendall, J.J.,
597 2017. Neogene shortening and exhumation of the Zagros fold-thrust belt and foreland
598 basin in the Kurdistan region of northern Iraq. Tectonophysics 694, 332–355.
599 Kottek, M., Grieser, Jj., Beck, C., Rudolf, B.,Rubel, F., 2006. World Map of the Koppen-
600 Geiger climate classification updated. Meteorologische Zeitschrift 15, 259–263.
601 Lacombe, O., Mouthereau, F., Kargar, S., Meyer, B., 2006. Late Cenozoic and modern stress
602 fields in the western Fars (Iran): implications for the tectonic and kinematic evolution of
603 central Zagros. Tectonics 25, TC1003. doi:10.1029/2005TC001831.
604 Lacombe, O., Bellahsen, N. and Mouthereau, F., 2011. Fracture patterns in the Zagros Simply
605 Folded Belt (Fars, Iran): constraints on early collisional tectonic history and role of
606 basement faults. Geological Magazine 148, 940-963.
607 Langbein, W. B. et al., 1947. Topographic characteristics of drainage basins. United States
608 Geological Survey,W.-S. Paper 968-C, 125-157.
609 Larue, J.P., 2008. Effects of tectonics and lithology on long profiles of 16 rivers of the
610 southern Central Massif border between the Aude and the Orb (France). Geomorphology
611 93, 343–367. doi:10.1016/j.geomorph.2007.03.003.
612 Lavé, J., Avouac, J., 2000. Active folding of fluvial terraces across the Siwaliks Hills,
613 Himalayas of central Nepal. Journal of Geophysical Research 105, 5735-5770.
614 Masson, F., Chery, J., Hatzfeld, D., Martinod, J., Vernant, P., Tavakoli, F., Ghafory-Ashtiani,
615 M., 2005. Seismic versus aseismic deformation in Iran inferred from earthquakes and
616 geodetic data. Geophysical Journal International 160, 217-226.
617 McQuarrie, N., 2004. Crustal scale geometry of the Zagros fold-thrust belt, Iran. Journal of

618 Structural Geology 26, 519–535.
619 McQuarrie, N., van Hinsbergen, D. 2013. Retrodeforming the Arabia-Eurasia collision zone:
620 Age of collision versus magnitude of continental subduction. Geology 41, 315–318.
621 doi:10.1130/G33591.1.
622 Miller, S.R., Baldwin, S.L., Fitzgerald, P.G., 2012. Transient fluvial incision and active
623 surface uplift in the Woodlark Rift of eastern Papua New Guinea. Lithosphere 4, 131–
624 149. doi:10.1130/L135.1.
625 Molin, P., Pazzaglia, F.J., Dramis, F., 2004. Geomorphic expression of active tectonics in a
626 rapidly-deforming forearc, Sila massif, Calabria, southern Italy. American Journal of
627 Science 304, 559-589.
628 Montgomery, D.R., Foufoula-Georgiou, E., 1994. Channel network source representation
629 using digital elevation models. Water Resources Research. 29, 3925–3934.
630 Moosdorf, N., Cohen, S., von Hagke, C., 2018. A global erodibility index to represent
631 sediment production potential of different rock types. Applied Geography 101, 36-44.
632 Morell, K.D., Kirby, E., Fisher, D.M., Van Soest, M., 2012. Geomorphic and exhumational
633 response of the Central American Volcanic Arc to Cocos Ridge subduction. Journal of
634 Geophysical Research: Solid Earth 117. doi:10.1029/2011JB008969.
635 Mouthereau, F., Lacombe, O., Meyer, B., 2006. The Zagros folded belt (Fars, Iran):
636 constraints from topography and critical wedge modelling. Geophysical Journal
637 International 165, 336-356.
638 Mouthereau, F., Tensi, J., Bellahsen, N., Lacombe, O., De Boisgrollier, T., Kargar, S., 2007.
639 Tertiary sequence of deformation in a thin-skinned/thick-skinned collision belt: The
640 Zagros folded belt (Fars, Iran). Tectonics 26, Tc5006, doi: 10.1029/2007tc002098.
641 Mouthereau, F., Lacombe, O., Vergés, J., 2012. Building the Zagros collisional orogen:
642 timing, strain distribution and the dynamics of Arabia/Eurasia plate convergence.
643 Tectonophysics 532, 27–60.
644 Nissen, E., Tatar, M., Jackson, J.A., Allen, M.B., 2011. New views on earthquake faulting in
645 the Zagros fold-and-thrust belt of Iran. Geophysical Journal International 186, 928–944.
646 Obaid, A., Allen, M.B., 2017. Landscape maturity, fold growth sequence and structural style
647 in the Kirkuk Embayment of the Zagros, northern Iraq. Tectonophysics 717, 27–40.
648 Olivetti, V., Cyr, A.J., Molin, P., Faccenna, C., Granger, D.E., 2012. Uplift history of the Sila
649 Massif, southern Italy, deciphered from cosmogenic ^{10}Be erosion rates and river
650 longitudinal profile analysis. Tectonics 31, 1–19, doi:10.1029/2011TC003037.
651 Perotti, C., Chiariatti, L., Bresciani, I., Cattaneo, L., Toscani, G., 2016. Evolution and timing

652 of salt diapirism in the Iranian sector of the Persian Gulf. Tectonophysics 679, 180–198.
653 Phillips, J.D., Lutz, J.D., 2008. Profile convexities in bedrock and alluvial streams.
654 Geomorphology 102, 554–566, doi:10.1016/j.geomorph.2008.05.042.
655 Pike, R. J., Wilson, S. E., 1971. Elevation-relief ratio, hypsometric integral, and
656 geomorphicarea-altitude analysis. Bulletin of the Geological Society of America 82,
657 1079–1084.
658 Ramsey, L. A., Walker, T., Jackson, J., 2008. Fold evolution and drainage development in the
659 Zagros mountains of Fars province, SE Iran. Basin Research 20, 23–48.
660 Ruh, J.B., Hirt, A.M., Burg, J.P., Mohammadi, A., 2014. Forward propagation of the Zagros
661 Simply Folded Belt constrained from magnetostratigraphy of growth strata. Tectonics
662 33, 1534-1551.
663 Schildgen, T.F., Cosentino, D., Bookhagen, B., Niedermann, S., Yildirim, C., Echtler, H.,
664 Wittmann, H., Strecker, M.R., 2012. Multi-phased uplift of the southern margin of the
665 Central Anatolian plateau, Turkey: A record of tectonic and upper mantle processes.
666 Earth and Planetary Science Letters 317–318, 85–95. doi:10.1016/j.epsl.2011.12.003.
667 Schumm, S.A., 1956. Evolution of drainage systems and slopes in badlands at Perth Amboy,
668 New Jersey. Bulletin of the Geological Society of America 67, 597–646.
669 Schwanghart, W. and Scherler, D., 2014. TopoToolbox 2–MATLAB-based software for
670 topographic analysis and modeling in Earth surface sciences. Earth Surface Dynamics 2,
671 1-7.
672 Scotti, V.N., Molin, P., Faccenna, C., Soligo, M. and Casas-Sainz, A., 2014. The influence of
673 surface and tectonic processes on landscape evolution of the Iberian Chain (Spain):
674 Quantitative geomorphological analysis and geochronology. Geomorphology 206, 37-57.
675 Seeber, L., Gornitz, V., 1983. River profiles along the Himalayan arc as indicators of active
676 tectonics. Tectonophysics 92, 335341–337367.
677 Shahzad, F., Gloaguen, R., 2011. TecDEM: A MATLAB based toolbox for tectonic
678 geomorphology, part 1: drainage network preprocessing and stream profile analysis.
679 Computers and Geosciences 37, 250–260.
680 Sissakian, V.K., 2000. Geological Map of Iraq, Geological Survey and Mining, Baghdad,
681 Iraq, Scale 1:1,000,000.
682 Stern, R. J., Johnson, P., 2010. Continental lithosphere of the Arabian Plate: A geologic,
683 petrologic, and geophysical synthesis. Earth-Science Reviews 101, 29–67.
684 Strahler, A., 1952. Hypsometric (area-altitude) analysis of erosional topology. Bulletin of the
685 Geological Society of America 63, 1117–1142.

686 Snyder, N.P., Whipple, K.X., Tucker, G.E., Merritts, D.J., 2000. Stream profiles in the
687 Mendocino triple junction region, northern California. Bulletin of the Geological Society
688 of America 112, 1250–1263. doi:10.1130/0016-7606(2000)112<1250:lrttfd>2.3.co;2.
689 Talbot, C.J., Alavi, M., 1996. The past of a future syntaxis across the Zagros, in Alsop. In:
690 Alsop, G.I., Blundell, D.J., Davison, I. (Eds.), Salt Tectonics. Geological Society,
691 London, Special Publications, 100, pp. 89–109. doi:10.1144/GSL.SP.1996.100.01.08. 1.
692 Talebian, M., Jackson, J., 2004. A reappraisal of earthquake focal mechanisms and active
693 shortening in the Zagros mountains of Iran. Geophysical Journal International 156, 506–
694 526.
695 Tucker, G.E., Whipple, K.X., 2002. Topographic outcomes predicted by stream erosion
696 models: sensitivity analysis and inter-model comparison. Journal of Geophysical
697 Research: Solid Earth 107, doi: 10.1029/2001JB000162.
698 Vergés, J., Saura, E., Casciello, E., Fernandez, M., Villasenor, A., Jimenez-Mount, I., Garcia-
699 Castellanos, D., 2011. Crustal-scale cross-sections across the NW Zagros belt:
700 implications for the Arabian margin reconstruction. Geological Magazine 148, 739–761.
701 Vernant, P., Nilforoushan, F., Hatzfel, D., Abbassi, M. R., Vigny, C., Masson, F., Nankali,
702 H., Matinod, J., Ashtiani, A., Bayer, R., Tavakoli, F., Chery, J., 2004. Present-day crustal
703 deformation and plate kinematics in the Middle East constrained by GPS measurements
704 in Iran and northern Oman. Geophysical Journal International 157, 381–398.
705 Walcott, R., Summerfield, M, 2008. Scale dependence of hypsometric integrals: An analysis
706 of southeast African basins. Geomorphology 96, 174–186.
707 Walker, R. T., Ramsey, L. A., Jackson, J., 2011. Geomorphic evidence for ancestral drainage
708 patterns in the Zagros Simple Folded Zone and growth of the Iranian plateau. Geological
709 Magazine 148, 901-910.
710 Whipple, K.X., Tucker, G.E., 1999. Dynamics of the stream-power river incision model:
711 Implications for height limits of mountain ranges, landscape response timescales, and
712 research needs. Journal of Geophysical Research 104, 17,661–17,674.
713 Whipple, K.X., Tucker, G.E., 2002. Implications of sediment-flux dependent river incision
714 models for landscape evolution. Journal of Geophysical Research 107 (B2), doi:
715 10.1029/2000JB000044.
716 Whipple, K.X., 2004. Bedrock Rivers and the Geomorphology of Active Orogens. Annual
717 Revew of Earth Planetary Science 32, 151–185.
718 Whittaker, A.C., Cowie, P. A., Attal, M., Tucker, G. E., Roberts, G. P., 2007. Contrasting
719 transient and steady-state rivers crossing active normal faults: new field observations

720 from the Central Apennines, Italy. Basin Research 19, 529–556.
721 Whittaker. A.C., Attal, M, Cowie, P. A., Tucker, G. E., Roberts, G., 2008. Decoding temporal
722 and spatial patterns of fault uplift using transient river long profiles. Geomorphology
723 100, 506–526.
724 Whittaker, A.C., Boulton, S.J., 2012. Tectonic and climatic controls on knickpoint retreat
725 rates and landscape response times. Journal of Geophysical Research: Earth Surface
726 117, F02024.
727 Wobus, C.W., Hodges, K. V., Whipple, K.X., 2003. Has focused denudation sustained active
728 thrusting at the Himalayan topographic front? Geology 31, 861–864.
729 Wobus, C., Whipple, K.X., Kirby, E., Snyder, N., Johnson, J., Spyropolou, K., Crosby, B.,
730 Sheehan, D., 2006 . Tectonics from topography: procedurses, promise, and pitfalls.
731 Special papers-Geological Society of America 398, 55–74. doi:10.1130/2006.2398(04).
732 Wohl, E. E., Merritt, D. M., 2001. Bedrock channel morphology. Geological Society of
733 America Bulletin 113, 1205–1212.
734 Zebari, M.M. and Burberry, C.M., 2015. 4-D evolution of anticlines and implications for
735 hydrocarbon exploration within the Zagros Fold-Thrust Belt, Kurdistan Region, Iraq.
736 GeoArabia 20, 161-188.
737 Zielke, O., Arrowsmith, J.R., Ludwig, L.G., Akçiz, S.O., 2010. Slip in the 1857 and earlier
738 large earthquakes along the Carrizo Plain, San Andreas Fault. Science 327, 1119-1122.
739